Magnetospheric radio tomographic imaging with IMAGE and Wind

Y. Zhai,[1] S. A. Cummer,[2] J. L. Green,[3] B. W. Reinisch,[4] M. L. Kaiser,[5] M. J. Reiner,[6,7] and K. Goetz[8]

Received 13 April 2011; revised 22 September 2011; accepted 28 September 2011; published 10 December 2011.

[1] Recent theoretical studies have shown the feasibility and potential scientific value of radio tomographic imaging of Earth's magnetosphere by measuring Faraday rotation and phase difference (or group delay) of coherent radio wave signals. On 15 August 2000, a 6 W linearly polarized 828 kHz signal transmitted by the Radio Plasma Imager (RPI) on the IMAGE spacecraft was clearly detected by WAVES X and Z antennas on Wind spacecraft. Following our previous analysis of the path-integrated product change of the magnetic field and plasma density based on the spin rate measurement, we report here Faraday rotation measured from absolute antenna orientation using the phase difference between the spin-phase modeled RPI signal and the WAVES X- and Z-antenna received RPI signals. The new approach gives Faraday rotation without the mod (π) ambiguity. The average electron density extracted along a typical signal propagation path over a 1 hour measurement window agrees well with empirical models of the northern polar region derived from years of measurements. Finally, we demonstrate preliminary 2-D radio tomographic imaging of magnetospheric plasma density using the Faraday rotation measurement.

Citation: Zhai, Y., S. A. Cummer, J. L. Green, B. W. Reinisch, M. L. Kaiser, M. J. Reiner, and K. Goetz (2011), Magnetospheric radio tomographic imaging with IMAGE and Wind, *J. Geophys. Res.*, *116*, A12208, doi:10.1029/2011JA016743.

1. Introduction

[2] Radio tomography has been successfully used over the past decade to measure ionospheric structure by integrated line-of-sight measurements [*Fougere*, 1995; *Walker et al.*, 1996; *Sutton and Na*, 1996; *Kamalabadi et al.*, 1999; *Pryse*, 2003]. It has also been shown in recent years to be a new promising technique in remote sensing Earth's magnetosphere [*Reinisch et al.*, 1999; *Ergun et al.*, 2000; *Ganguly et al.*, 2000; *Cummer et al.*, 2001; *Zhai and Cummer*, 2005, 2006]. Magnetospheric radio tomographic imaging uses radio waves and phenomena known as Faraday rotation or group delay that can be measured to reconstruct full images of Earth's electron density and magnetic field. The ability to accurately image electron density on a large scale from simultaneous measurements of group delay (or phase difference) and Faraday rotation of two coherent radio signals would be a major advance for magnetospheric science to address many currently unanswered fundamental questions [*Ergun et al.*, 2000].

[3] Two distinct forms have been proposed in recent theoretical studies for imaging Earth's magnetosphere with radio tomography [*Ergun et al.*, 2000; *Ganguly et al.*, 2000]. One is to image electron density from the Total Electron Content (TEC) measurements from either phase difference or group delay of two radio signals [*Ergun et al.*, 2000]. The other is a combined reconstruction of the electron density N_e and the magnetic field $\boldsymbol{B}$ from TEC and Faraday rotation measurements [*Ganguly et al.*, 2000]. In addition to popular iterative approaches, a direct reconstruction method was also introduced for magnetospheric radio tomographic imaging [*Zhai and Cummer*, 2005, 2006]. The main advantage of a direct method is that extra information, such as in situ measurements, can be easily incorporated into an image reconstruction process. The good performance of this method was demonstrated in reconstructing electron density and magnetic field using MHD model simulated constellations of relatively few satellites (11 and fewer) in a single orbit in a variety of magnetospheric regions.

[4] Remote sensing techniques based on TEC measurements have been widely used for imaging the ionospheric electron density distribution [*Raymund et al.*, 1990; *Na et al.*, 1995; *Ganguly et al.*, 2000]. The concept of imaging

[1]Princeton Plasma Physics Laboratory, Princeton University, Princeton, New Jersey, USA.
[2]Electrical and Computer Engineering Department, Duke University, Durham, North Carolina, USA.
[3]Planetary Sciences Division, NASA Headquarters, Washington, DC, USA.
[4]Center for Atmospheric Research, University of Massachusetts, Lowell, Massachusetts, USA.
[5]Space Weather Laboratory, NASA Goddard Space Flight Center, Greenbelt, Maryland, USA.
[6]Institute for Astrophysics and Computational Sciences, Catholic University of America, Washington, DC, USA.
[7]NASA Goddard Space Flight Center, Greenbelt, Maryland, USA.
[8]School of Physics and Astronomy, University of Minnesota, Minneapolis, Minnesota, USA.

Copyright 2011 by the American Geophysical Union.
0148-0227/11/2011JA016743

magnetospheric electron density with TEC measurements has been proven in a single propagation path experiment with spacecraft ISEE 1 and 2, which contained a transmitter-receiver pair designed to measure the total phase shift on a 683 kHz signal propagating between the two spacecraft [*Harvey et al.*, 1978]. While the phase difference and group delay provide integrated measurements of electron density only, Faraday rotation provides global information about the product of the magnetic field and electron density and is therefore sensitive to changes in both quantities. The experimental implementation of measuring Faraday rotation for magnetospheric radio tomographic imaging has, however, not been pursued until recently.

[5] The Wind experiment in 2000 successfully measured the change of path-integrated product of magnetospheric parameters on a signal transmitted from the Radio Plasma Imager (RPI)[*Reinisch et al.*, 2000]; the radio signal from the Imager for Magnetopause-to-Aurora Global Exploration (IMAGE) was received by the WAVES receivers [*Bougeret et al.*, 1995] on the Wind satellite [*Cummer et al.*, 2001]. A preliminary analysis has demonstrated measurability of Faraday rotation of the transmitted electric field waveforms from the time-varying spin modulation of the WAVES received RPI signal [*Cummer et al.*, 2001]. The results provided a global measurement of path-integrated product of magnetospheric parameters, thereby providing an initial validation of the radio tomography concept. However, the total Faraday rotation that is physically more meaningful, and the path-averaged electron density that is scientifically more valuable to a true radio tomographic imaging mission, can not be extracted from the previous analysis using the spin rate measurement.

[6] In this paper, we use absolute antenna orientation based on spacecraft spin-axis and spin-phase data to complete our previous analysis of the IMAGE and Wind experiment. The new approach gives the total Faraday rotation of the RPI signal in a way that allows removal of the mod (π) ambiguity, and both the X- and Z-antenna received signals are used for a consistency check of the polarity of the Faraday rotation and the spin period change. We first compare the spin phase difference between a model predicted RPI signal with actual IMAGE spin phase but zero Faraday rotation and the WAVES received RPI signal with measured time-varying spin modulation. We then extract the path-integrated electron density from the Faraday rotation measurements, and compare the deduced average electron density with empirical models. Finally, we demonstrate basic radio tomographic imaging by reconstructing a 2-D electron density image with an assumption of the density distribution along signal propagation paths.

2. Theoretical Background

[7] The idea of the IMAGE and Wind experiment is to test the concept of magnetospheric radio tomography using Faraday rotation measurement. Faraday rotation is the rotation of the plane of polarization of a linearly polarized wave as it travels through a magnetized medium such as the magnetospheric plasma. A linearly polarized wave can be decomposed into two circularly polarized waves of equal amplitude, rotating in opposite direction. At any point in space the sum of the two circularly polarized waves produces a linearly polarized wave the polarization of which varies along the path. Due to a difference in the propagation constant or phase velocity for the right-hand (RH) and left-hand (LH) polarized waves, the plane of polarization rotates as the wave propagates through the magnetosphere under the influence of Earth's magnetic field. Faraday rotation is the rotation of the linear polarization when the component waves propagate over a distance d

$$\theta_F = \int_0^d \frac{\beta_{LH}(s) - \beta_{RH}(s)}{2} ds = \int_0^d \frac{\omega\sqrt{\mu_0\epsilon_{LH}} - \omega\sqrt{\mu_0\epsilon_{RH}}}{2} ds, \tag{1}$$

where β_{LH} and β_{RH} are wave propagation constants. The effective dielectric permittivities for the LH and RH waves are

$$\epsilon_{LH} = \epsilon_0\left\{1 - \frac{\omega_p^2}{\omega(\omega_c + \omega)}\right\}; \quad \epsilon_{RH} = \epsilon_0\left\{1 + \frac{\omega_p^2}{\omega(\omega_c - \omega)}\right\}, \tag{2}$$

where $\omega_p = \sqrt{\frac{N_e q_e^2}{m_e \epsilon_0}}$ is the plasma oscillation frequency due to electron vibration, and $\omega_c = -\frac{q_e}{m_e}B_0$ the plasma gyrofrequency due to magnetic field B_0 parallel to the direction of wave propagation. For frequencies higher than the plasma frequency and gyrofrequency, the resulting Faraday rotation implies a concurrent measurement of the electron density and the parallel magnetic field. Faraday rotation is thus directly proportional to the product of the electron density and the parallel magnetic field

$$\theta_F = K \int_0^d N_e\left(\hat{\boldsymbol{k}} \cdot \boldsymbol{B}\right) ds \tag{3}$$

where $\hat{\boldsymbol{k}}$ is the normalized wave direction vector along the propagation path, and $K = q^3(2\epsilon_0 c m_e^2 \omega^2)^{-1}$ a frequency dependent parameter [*Budden*, 1985, p. 374; *Inan and Inan*, 2000, p. 459].

[8] Faraday rotation and TEC measurements from either phase difference or group delay of two coherent radial signals are the primary parameters needed for tomographically reconstructing full images of Earth's magnetosphere. With a magnetic field model, the path-integrated electron density can be reconstructed from a Faraday rotation measurement.

3. The IMAGE and Wind Experiment

[9] A preliminary analysis of the IMAGE and Wind experiment demonstrated measurability of Faraday rotation and thus feasibility of magnetospheric radio tomographic imaging [*Cummer et al.*, 2001]. We first review the experiment for completeness of this paper. From 19.5 to 23.5 UT on August 15, 2000, the IMAGE spacecraft periodically transmitted a linearly polarized 828 kHz single frequency signal from one of its spinning dipole antennas. The radio transmission went through 120 second cycles of 64 s alternating 0.5 second on and 0.5 s off modulation, then 56 s of silence. The RPI signal was clearly detected by both WAVES spinning dipole (X-antenna), which has a 3 second spin period and stationary dipole (Z-antenna) on Wind. A

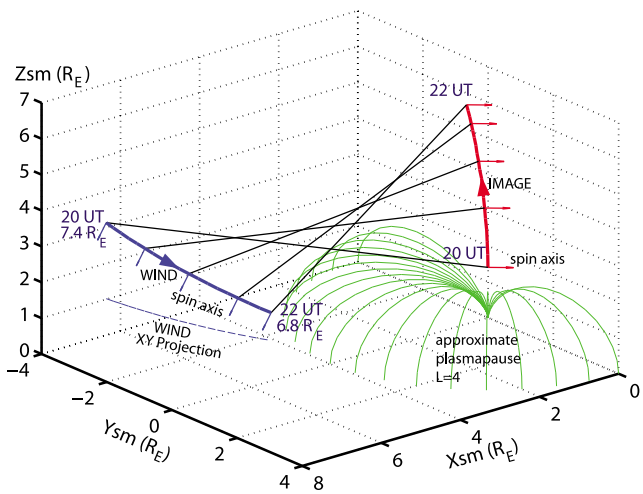

Figure 1. The IMAGE and Wind trajectories and RPI signal propagation paths between spacecraft from 20.0-22.0 UT on 15 August 2000. The $L = 4$ surface is the plasmapause location estimated from a magnetic field model to indicate that propagation paths during the time intervals are outside the plasmapause.

close look at the transmitted and received RPI signals indicated a difference in spin-induced signal modulation due to the time-varying Faraday rotation over signal propagation paths [*Cummer et al.*, 2001]. Figure 1 shows the IMAGE and Wind trajectories and spin axes during the experiment from 20.0 to 22.0 UT on 15 August 2000. The probed region in this experiment is clearly outside the plasmasphere and the propagation paths do not intersect the plasmapause boundary. Therefore, it is the relatively high latitude plasma that we are measuring and imaging using basic reconstruction techniques.

[10] Figure 2 presents the received RPI signal by the Wind X and Z antennas during the experiment. The main feature observed in both antenna signals is the 64 second on and 56 second off modulation from the transmitter modulation. The 0.5 s on and 0.5 s off fast transmitter modulation is responsible for the slightly noisy appearance of each 64 second "on" period. A careful examination of the signals shows that the signal amplitude is slowly varying across each 64 second "on" period. This is produced by the 122.7 second spin period of the transmitting antenna and thus the slow modulation of the transmitted wave polarization. This is more easily seen in Figure 3, where it is also seen that signal minima in one antenna correspond to signal maxima in the other antenna, as expected for orthogonal antennas and a rotating wave polarization. Additional fast modulation of the X antenna signal is produced by the 3 second spin period of the Wind spacecraft, but this has minimal impact on the measurements.

[11] Figure 3 presents the measured spin modulation of the WAVES antenna received signals. The measurement is performed by matching the nulls of a continuously fit spin period for a modeled signal to the measured signal nulls [*Cummer et al.*, 2001]. Although it is shown for a small time window for clarity, the fitting of the spin modulation is performed over the whole time window. The received signal spin modulation from both antennas initially shows a spin period over 30 percent larger than the 122.7 second actual IMAGE spin period but the spin period reduces considerably from 20.1 to 20.5 UT, then slowly reduces to the actual IMAGE spin period from 20.5 to 21.0 UT and stays almost unchanged from 21.0 to 23.0 UT toward the end of the experiment. This spin period discrepancy implies Faraday rotation change on signal propagation paths and the change of the path-integrated product of electron density and parallel magnetic field as measured by [*Cummer et al.*, 2001]. There is, however, ambiguity in measuring total Faraday rotation by the spin rate-based approach. Further analysis is needed to extract electron density distribution along propagation paths for a real test of magnetospheric radio tomographic imaging.

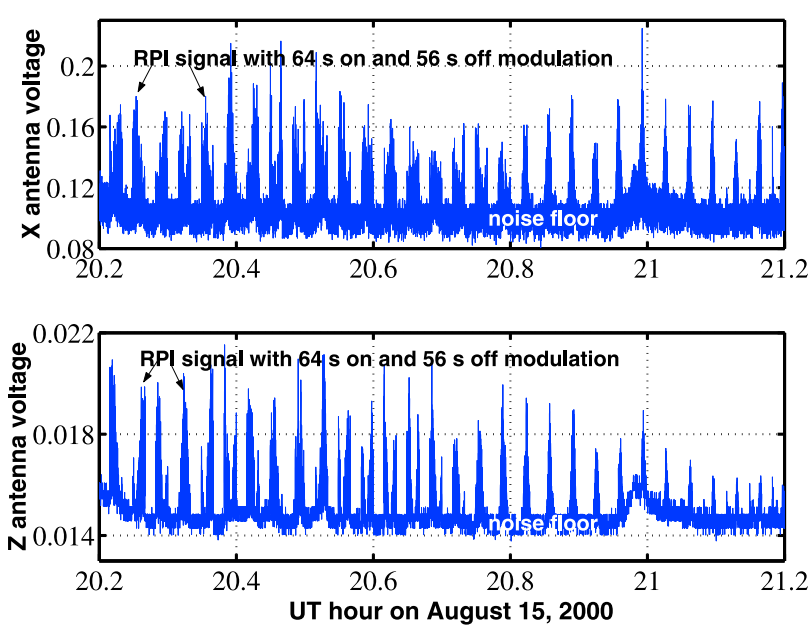

Figure 2. The WAVES X and Z antenna received RPI signals ($nV/\sqrt{Hz}$).

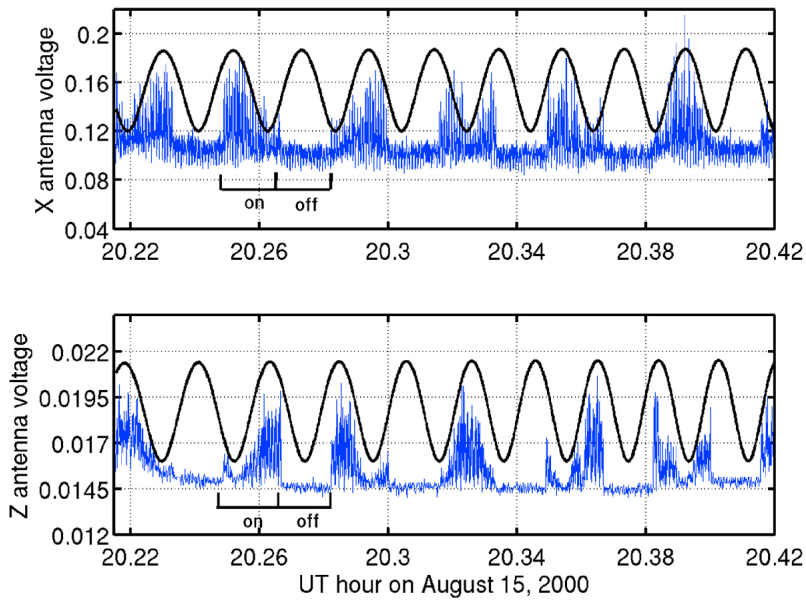

Figure 3. The fit spin modulation of WAVES received RPI signals.

[12] We use absolute IMAGE and Wind antenna orientations based on spacecraft spin-axis and spin phase data to measure the total Faraday rotation without the mod (π) ambiguity. The absolute antenna orientation gives spin phase difference between the modeled RPI signal with the actual IMAGE spin phase but no Faraday rotation, and the WAVES received signals with fit spin modulation and time-varying Faraday rotation. The modeled signals are obtained using IMAGE and Wind spacecraft locations during the experiment and the actual IMAGE spin phase data are obtained from NASA's CDA Web site http://cdaweb.gsfc.nasa.gov.

4. Faraday Rotation Measurements

[13] In the preliminary analysis *Cummer et al.* [2001] successfully measured the change in the path-integrated product of electron density and magnetic field from the time-varying Faraday rotation by measuring the spin rate change of the observed RPI signal but with an undetermined initial constant that is difficult to choose. As a first attempt for real magnetospheric tomographic imaging, we use the absolute antenna orientation and the Wind perceived IMAGE spin phase shift to measure Faraday rotation. Specifically, Faraday rotation $\theta_F(t)$ is the spin phase difference between the received signal with measurable time-varying spin modulation and the modeled signal with uniform spin modulation using the actual IMAGE spin-phase

$$\Lambda_{PEV}(t) = \Lambda_{RPI}(t) + \theta_F(t), \tag{4}$$

where $\Lambda_{PEV}(t)$ and $\Lambda_{RPI}(t)$ are the spin phase angles of the WAVES received and the IMAGE spin-phase modeled RPI signals, respectively. The IMAGE spin phase data is downloaded from NASA's CDA Web site. To obtain the WAVES received signal spin modulation, we iteratively compute a smooth spin period $T_{PEV}(t)$ that fits the nulls and maxima of the times of the measured signal nulls and maxima. The spin phase of the received signal is computed from the perceived time-varying spin period

$$\Lambda_{PEV}(t) = \int_0^t \frac{2\pi}{T_{PEV}(\tau)} d\tau + \phi_0, \tag{5}$$

where ϕ_0 is the initial phase as a result of iterative fitting. The signal with measured spin modulation is obtained by projecting the perceived instantaneous IMAGE antenna orientation $\hat{\boldsymbol{r}}_{PEV}$ computed from $\Lambda_{PEV}(t)$ onto the plane orthogonal to the propagation path first, and next projecting the resulting transverse field direction onto the known WAVES receiving antenna direction $\hat{\boldsymbol{r}}_{WAV}$.

$$S_{pev} \propto \hat{\boldsymbol{k}} \times \left(\hat{\boldsymbol{r}}_{PEV} \times \hat{\boldsymbol{k}}\right) \cdot \hat{\boldsymbol{r}}_{WAV}. \tag{6}$$

Likewise, the modeled signal with zero Faraday rotation is obtained by projecting the instantaneous IMAGE antenna orientation $\hat{\boldsymbol{r}}_{RPI}$ obtained from actual spin phase data, onto the plane orthogonal to signal propagation path first, and next projecting the resulting transverse field direction onto the WAVES receiving antenna direction.

$$S_{src} \propto \hat{\boldsymbol{k}} \times \left(\hat{\boldsymbol{r}}_{RPI} \times \hat{\boldsymbol{k}}\right) \cdot \hat{\boldsymbol{r}}_{WAV}. \tag{7}$$

Faraday rotation is the spin phase difference between the two signals S_{pev} and S_{src}. Figure 4 shows the difference between predicted signal with zero Faraday rotation and the observed signal with measured spin modulation from the WAVES X and Z antenna. The clear spin modulation discrepancy shown in Figure 4 suggests measurable Faraday rotation along the IMAGE to Wind propagation paths. The spin phase of the observed signals from both X and Z antenna leads the model predicted signal with zero Faraday rotation. This implies a negative Faraday rotation along the propagation path and it is consistent with the direction of the parallel magnetic field shown in Figure 6. The time-varying

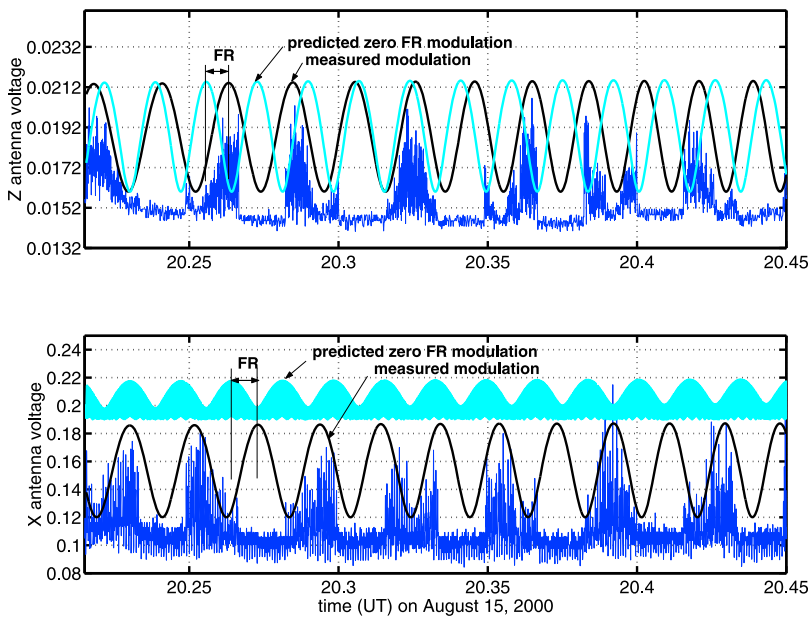

Figure 4. Predicted RPI signal with zero Faraday Rotation (FR) and WAVES received RPI signal with measurable non-zero FR.

Faraday rotation directly contains valuable information of the spatially varying magnetospheric medium between the two spacecraft.

[14] The measured Faraday rotation from the WAVES X antenna signal is shown in Figure 5, where the $\pm(n\pi)$ ambiguity can be resolved because we expect a close to zero Faraday rotation after 21.0 UT as shown in the thick line in Figure 5. The Faraday rotation measured from the Z antenna signal during 20.0-20.6 UT is the same as that measured from the X antenna signal, but the Z antenna signal is not reliable after 20.8 UT due to a lower SNR that obscured the spin modulation. Although the following analysis is based on Faraday rotation measured from the X antenna signal, the spin period from both X- and Z-antenna signals in Figure 3 is consistent in that it is initially about 30 percent larger than the actual IMAGE spin period but reduces considerably from 20.1 to 20.5 UT.

[15] The magnetic field in Earth's magnetosphere has been studied for decades [*Tsyganenko and Stern*, 1996; *Tsyganenko*, 2002]. To extract a path-averaged electron density, we use the Tsyganenko model downloaded from NASA Web site as the background magnetic field. The direction vector $\hat{\boldsymbol{k}}$ is obtained from IMAGE and Wind locations also available at the CDA Web site. The parallel magnetic field is shown in Figure 6.

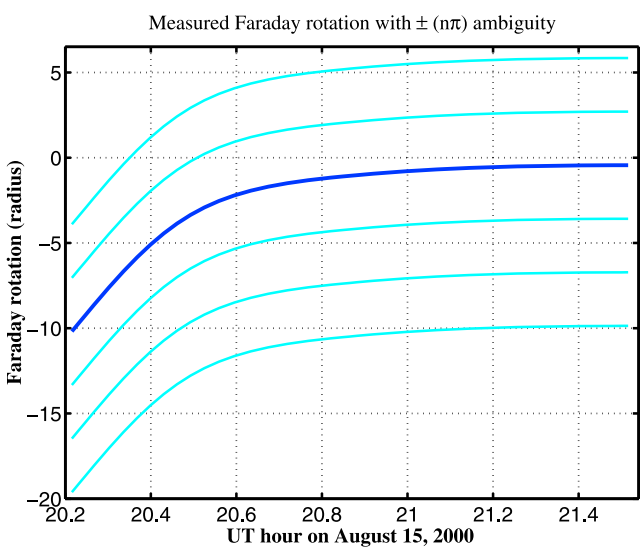

Figure 5. The family of Faraday rotation from WAVES X-antenna received RPI signals with time-varying modulation. The mod (π) ambiguity is removed (thick blue line) because we expect a zero Faraday rotation after 21.0 UT.

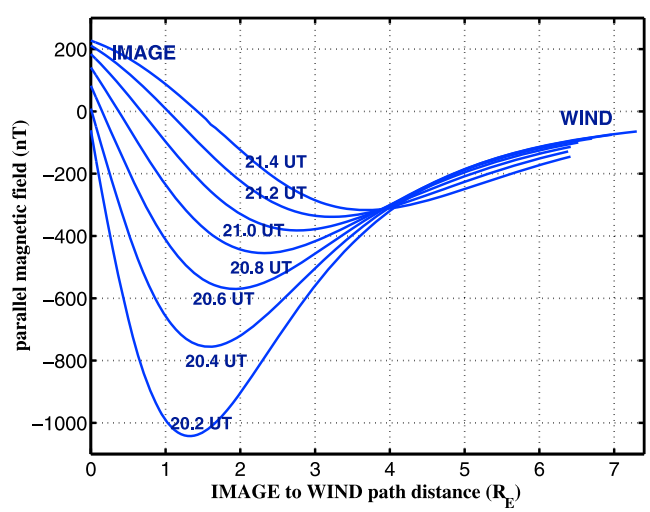

Figure 6. The parallel magnetic field along propagation path from IMAGE to Wind during 20.2-21.4 UT on 15 August 2000.

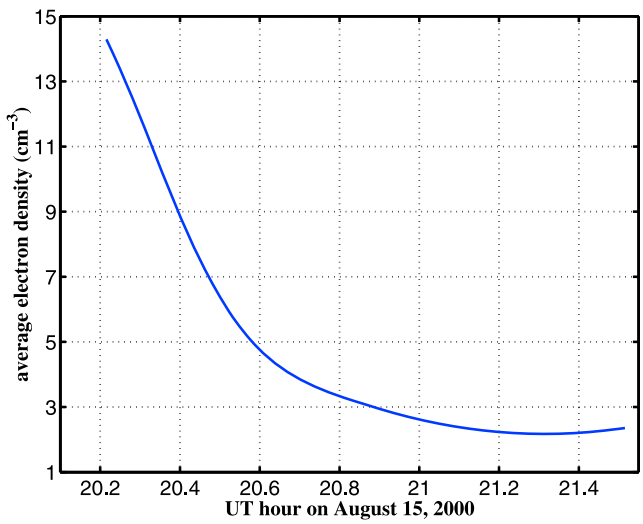

Figure 7. The parallel ***B***-averaged electron density along signal propagation paths.

[16] Information of the plasma density in the north polar region from the high-altitude ionosphere to the magnetosphere is central for characterizing the global structure and understanding the general dynamics of Earth's magnetosphere. Its spatial and temporal variations provide clues to the origin and evolution of numerous fundamental processes occurring in the polar region, such as the solar wind interaction with Earth's magnetosphere and the geomagnetic storms and substorms. Based on the Faraday rotation we measured, an averaged plasma density along wave propagation paths can be extracted from (3), with ***B*** approximated by the Tsyganenko model

$$\overline{N}_e = \frac{\theta_F}{K \sum_{i=1}^{n} (\hat{\boldsymbol{k}} \cdot \boldsymbol{B})_i ds_i}, \tag{8}$$

where n is the number of segments along each propagation path. The extracted path-averaged electron density is shown in Figure 7. The decreasing trend of $\overline{N}_e$ from 20.2 to 21.2 UT is consistent with the upward motion of IMAGE in the north polar region, which leads to a decreasing path-integrated electron density.

[17] The polar region electron density was first measured by *Persoon et al.* [1983] from the whistler mode upper-frequency cutoff with the plasma wave instrument (PWI) on the Dynamics Explorer 1 (DE 1) spacecraft. A power law exponent of -3.85 ± 0.32 dependence of N_e on radial distance has been found. The N_e distribution in the northern polar region has also been studied using RPI on IMAGE spacecraft over a five-month period from June 2000 to November 2001. As a result, a new statistical electron density model was introduced as a function of radial distance, solar illumination and geomagnetic activity [*Nsumei et al.*, 2008]. This latest model has been benchmarked against previous electron density models.

[18] To compare the average electron density extracted from our measured Faraday rotation with empirical models, we note from Figure 6 and equation (8) that the ***B***-averaged density $\bar{N}_e$ is closest to N_e at locations of the maximum parallel magnetic field along each propagation path, which is roughly $\frac{1}{5}$ of the path distance from IMAGE as shown in Figure 6. Observations from the National Geophysical Data Center show very quiet geomagnetic conditions with a global κ_p index of 1.7 during 18.0 to 21.0 UT on Aug 15, 2000, which means the electron density distribution in the magnetosphere does not change substantially during the time interval of our interest. We then compare the measured electron density with model predictions at these locations for quiet geomagnetic condition and an intermediate solar zenith angle [*Nsumei et al.*, 2008]. We assume that the N_e distribution follows the power law dependence on geocentric radial distance along each propagation path. Figure 8 shows that the reconstructed electron density agrees well with predictions from various models of northern polar region [*Persoon et al.*, 1983; *Nsumei et al.*, 2008]. We emphasize here that the measurements done by Nsumei and Persoon are the averaged electron density over a five-month period while our measurement was made in basically only one hour time frame.

5. Magnetospheric Tomographic Imaging

[19] If we further assume that the electron density in the probed region is independent of the azimuth angle ϕ as the propagation paths from IMAGE to Wind rotate azimuthally from 20.0 UT to 22.0 UT as shown in Figure 1, and the N_e distribution along each propagation path follows the functional dependence on geocentric radial distance as in the empirical model $N_e \propto \kappa(\theta)R^{\alpha}$, with $\alpha = -3.85$, we could reconstruct a 2-D image of N_e in the vertical RZ plane of the IMAGE and Wind probed region. Again, we assume here there is no significant change of electron density distribution in the magnetosphere based on the observation of very quiet geomagnetic conditions during 20.0-22 UT.

[20] The reconstruction is based on the path-integrated electron density $\bar{N}_e$, the parallel magnetic field $B_p = \hat{\boldsymbol{k}} \cdot \boldsymbol{B}$, and the radial distance R. Specifically, let $\{t_1\ t_2\ ..\ t_m\}$ be an ensemble of time frames from 20.2 to 21.5 UT on 15 August

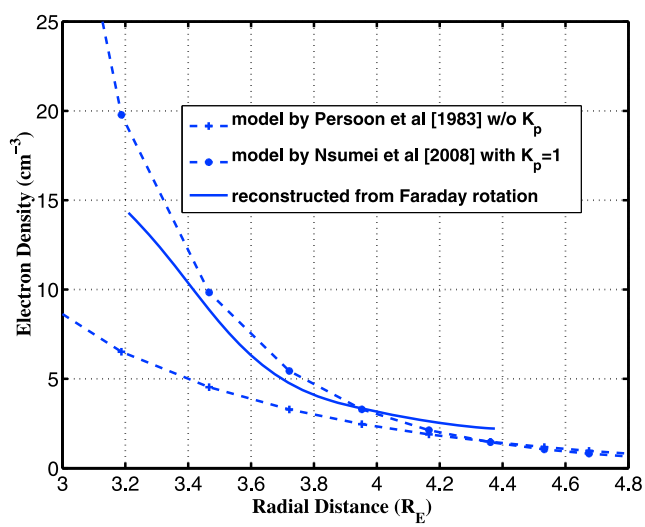

Figure 8. Comparison of reconstructed electron density against radius distance for positions with maximum parallel magnetic field along IMAGE to Wind paths.

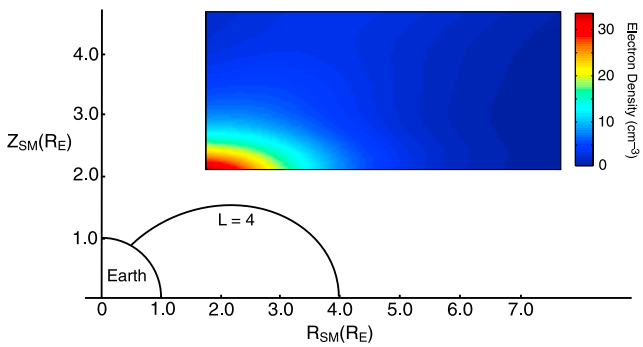

Figure 9. A reconstructed 2-D electron density image (in cm^{-3}) based on the measured total Faraday rotation. The image spatial resolution is 100 by 80.

2000; $\{R_1\ R_2\ ..\ R_n\}$ be the radial distances for a set of space points along each IMAGE to Wind path; $\{N_{e1}\ N_{e2}\ ..\ N_{en}\}$ be a set of electron density values along the propagation path at t_j, with $j = 1, .., m$, we then obtain

$$N_{e1} = \frac{R_1^{\alpha} \sum_{i=1}^{n} B_{pi} ds_i}{\sum_{i=1}^{n} B_{pi} ds_i R_i^{\alpha}} \overline{N}_{ej}, .., \quad N_{en} = \frac{R_n^{\alpha} \sum_{i=1}^{n} B_{pi} ds_i}{\sum_{i=1}^{n} B_{pi} ds_i R_i^{\alpha}} \overline{N}_{ej}, \qquad (9)$$

where ds_i is the length of the ith discrete segment along the jth propagation path, and $\overline{N}_{ej}$ is the path-averaged electron density obtained from (8) at time t_j.

[21] With the two spacecraft and the single frequency experiment, we now extract the electron density distribution along the propagation paths using (9). In this direct reconstruction technique, we use 80 propagation paths from 20.2 to 21.5 UT and 100 segments along each propagation path for the reconstruction. We demonstrate potential values of the magnetospheric radio remote sensing technique by reconstructing a 2-D electron density image in the plane of the XY projection R_{sm} of each signal propagation path and the spacecraft Z_{sm} coordinates. Figure 9 presents the reconstructed 2-D image of N_e distribution during the experiment. It clearly shows the spatially varying magnetospheric medium between the two spacecraft, and demonstrates the capabilities of magnetospheric radio tomographic imaging. The above measurements are feasible at relatively high latitudes and on large scale regions of space plasma over relatively long magnetospheric propagation paths. Global remote sensing of magnetospheric parameters based on the Faraday rotation measurement technique is of great interest to geospace scientists to answer fundamental questions regarding magnetospheric structure and dynamics.

[22] Compared to traditional tomographic problems widely used in medical applications, one practical constraint for radio tomographic imaging of the magnetosphere is that very few satellites are available for measurement, therefore we do not have the freedom to choose measurement raypaths crossing the region of interest and it is more ill-posed than the computer tomography in medical applications. Our previous studies show that for magnetospheric tomographic imaging a direct reconstruction method using fewer number of raypaths is more robust and it performs significantly better than popular iterative methods when the number of satellite is small [*Zhai and Cummer*, 2005].

[23] Since the electron density from above direct reconstruction is sensitive to a small parallel magnetic field along IMAGE to Wind propagation paths, uncertainty of the electron density in Figure 9 increases at a later UT time or higher altitudes. It is also noted that the statistical electron density model [*Nsumei et al.*, 2008] was established at a solar maximum, which is when our radio transmission for the tomographic imaging experiment was performed, a different electron density model may be needed if the above method is used again with a two-satellite radio transmission at different solar cycles or under non-quiet geomagnetic conditions. With the successful CLUSTER multispacecraft and dual-frequency radio transmissions for tomographic imaging of the magnetosphere [*Cummer et al.*, 2003], we hope to eliminate this limitation in future work. For non-quiet geomagnetic conditions, the direct reconstruction technique developed in our previous study [*Zhai and Cummer*, 2005, 2006] should be used with Faraday rotation measurements from multisatellites, dual-frequency radio transmission for better performance.

6. Conclusions

[24] On 15 August 2000, a 6 W and 828 kHz linearly polarized radio signal from RPI transmitter on IMAGE was observed by WAVES receivers on Wind. The time-varying spin modulation of the received signal waveform is clearly due to the time-varying Faraday rotation as the transmitted signal travels through Earth's magnetosphere. To complete the preliminary Faraday rotation analysis for radio tomographic imaging, we first extract the total Faraday rotation by computing the spin phase difference between the spin-phase predicted signal with zero Faraday rotation and the WAVES received signal with measured spin modulation and time-varying Faraday rotation. With the Tsyganenko magnetic field model, we then extract an average electron density over the signal propagation paths in the probed region and show that the deduced electron density agrees well with empirical models of the northern polar region. Finally, we demonstrate the radio tomographic imaging technique by reconstructing a 2-D electron density image of Earth's magnetosphere in the north polar region. Future investigation and application of this new remote sensing technique may provide valuable measurements to improve our understanding of large scale magnetospheric processes.

[25] **Acknowledgements.** This research was supported by NASA Geospace Sciences grant NNX07AGU14G.

[26] Philippa Browning thanks Robert MacDowall and another reviewer for their assistance in evaluating the paper.

References

Bougeret, J. L., et al. (1995), WAVES: The radio and plasma wave investigation on the Wind spacecraft, *Space Sci. Rev.*, *71*, 231–263.

Budden, K. G. (1985), *The Propagation of Radio Waves*, Cambridge Univ. Press, New York.

Cummer, S., M. Reiner, B. Reinisch, M. Kaiser, J. Green, R. Benson, R. Manning, and K. Goetz (2001), A test of magnetospheric radio tomographic imaging with IMAGE and Wind, *Geophys. Res. Lett.*, *28*(6), 1131–1134.

Cummer, S., et al. (2003), Advances in magnetospheric radio wave analysis and tomography, *Adv. Space Res.*, *32*(3), 329–336.

Ergun, R., et al. (2000), Feasibility of a multisatellite investigation of the Earth's magnetosphere with radio tomography, *J. Geophys. Res.*, *105*(A7), 361–373.

Fougere, P. (1995), Ionospheric radio tomography using maximum entropy: 1. Theory and simulation studies, *Radio Sci.*, *30*(2), 429–444.

Ganguly, S., G. Bavel, and A. Brown (2000), Imaging electron density and magnetic field distributions in the magnetosphere: A new technique, *J. Geophys. Res.*, *105*(A7), 16,063–16,081.

Harvey, C. C., J. Etcheto, J. D. Javel, R. Manning, and M. Petit (1978), The ISEE electron density experiment, *IEEE Trans. Geosci. Electron.*, *16*, 231–238.

Inan, U. S., and A. S. Inan (2000), *Electromagnetic Waves*, Prentice Hall, Upper Saddle River, N. J.

Kamalabadi, F., W. Karl, J. Semeter, D. Cotton, T. Cook, and S. Chakrabarti (1999), A statistical framework for space-based EUV ionospheric tomography, *Radio Sci.*, *34*(2), 437–447.

Na, H., J. Shen, and H. Lee (1995), A fourier domain technique for ionospheric tomography, *Radio Sci.*, *30*, 747–754.

Nsumei, P. A., B. W. Reinisch, P. Song, J. Tu, and X. Huang (2008), Polar cap electron density distribution from IMAGE radio plasma imager measurements: Empirical model with the effects of solar illumination and geomagnetic activity, *J. Geophys. Res.*, *113*, A01217, doi:10.1029/2007JA012566.

Persoon, A. M., D. A. Gurnett, and S. D. Shawhan (1983), Polar cap electron densities from DE 1 plasma wave observations, *J. Geophys. Res.*, *88*, 10,123–10,136.

Pryse, S. E. (2003), Radio tomography: A new experimental technique, *Surv. Geophys.*, *24*, 1–38.

Raymund, T. D., J. R. Austen, S. J. Franke, C. H. Lui, J. A. Klobuchar, and J. Stalker (1990), Application of computerized tomography to the investigation of ionospheric structures, *Radio Sci.*, *25*, 771–789.

Reinisch, B. W., G. S. Sales, D. M. Haines, S. F. Fung, and W. L. Taylor (1999), Radio wave active Doppler imaging of space plasma structures: Arrival angle, wave polarization, and Faraday rotation measurements with the radio plasma imager, *Radio Sci.*, *34*(6), 1513–1524.

Reinisch, B. W., et al. (2000), The Radio Plasma Imager investigation on the IMAGE spacecraft, *Space Sci. Rev.*, *91*, 319–359.

Sutton, E., and H. Na (1996), Ionospheric tomography using the residual correction method, *Radio Sci.*, *31*(3), 489–496.

Tsyganenko, N. A. (2002), A model of the near magnetosphere with a dawn-dusk asymmetry: 1. Mathematical structure, *J. Geophys. Res.*, *107*(A8), 1179, doi:10.1029/2001JA000219.

Tsyganenko, N. A., and D. P. Stern (1996), Modeling the global magnetic field of the large-scale Birkeland current systems, *J. Geophys. Res.*, *101*, 27,187–27,198.

Walker, I., J. Heaton, L. Kersley, C. Mitchel, S. Pryse, and M. Williams (1996), EISCAT verification in the development of ionospheric tomography, *Ann. Geophys.*, *14*, 1413–1421.

Zhai, Y., and S. A. Cummer (2005), A flexible and robust direct reconstruction method for magnetospheric radio tomography, *Radio Sci.*, *40*(3), RS3004, doi:10.1029/2004RS003100.

Zhai, Y., and S. A. Cummer (2006), An orthogonal projection and regularization technique for magnetospheric radio tomography, *J. Geophys. Res.*, *111*, A03207, doi:10.1029/2005JA011039.

S. A. Cummer, Electrical and Computer Engineering Department, Duke University, Box 90291, Durham, NC 27708, USA. (cummer@ee.duke.edu)

K. Goetz, School of Physics and Astronomy, University of Minnesota, Minneapolis, MN 55455, USA.

J. L. Green, Planetary Sciences Division, NASA Headquarters, 300 E St., SW, MS 3274, Washington, DC 20546-0001, USA.

M. L. Kaiser, Space Weather Laboratory, NASA Goddard Space Flight Center, Greenbelt, MD 20771, USA.

M. J. Reiner, NASA Goddard Space Flight Center, Greenbelt, MD 20771, USA.

B. W. Reinisch, Center for Atmospheric Research, University of Massachusetts, Lowell, MA 01854, USA.

Y. Zhai, Princeton Plasma Physics Laboratory, PO Box 451, Princeton University, Princeton, NJ 08543, USA. (yzhai@pppl.gov)